nature methods

Supplementary information

https://doi.org/10.1038/s41592-026-03213-8

Reconstructing signaling histories of single cells via perturbation screens and transfer learning

In the format provided by the authors and unedited

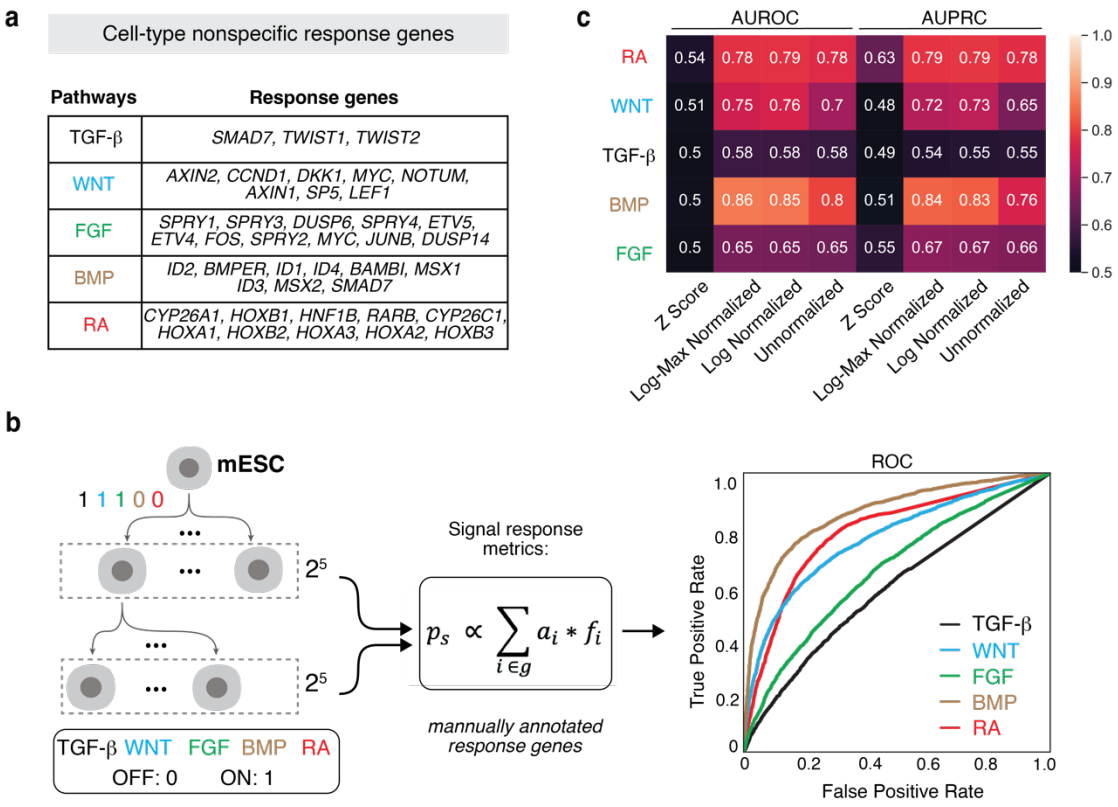

Supplementary Figure 1. Signal inference using the response-gene method.
a, A list of response genes chosen for each signaling pathway was modified from Han *et al*. 2020 [17]. **b**, Response genes inferred signaling pathway activities with limited accuracy, as tested with a ground-truth dataset of mESC differentiation [21]. Signaling states are represented as binary strings. The probability of being a responding cell (p_s) was computed as summed expression of response genes (f_i) with weights (a_i). ROC, receiver operating characteristic. **c**, The performance of the response-gene method for signal inference, computed based on different normalization strategies for gene expression. AUROC, area under the receiver operating curve; AUPRC, area under the precision recall curve.

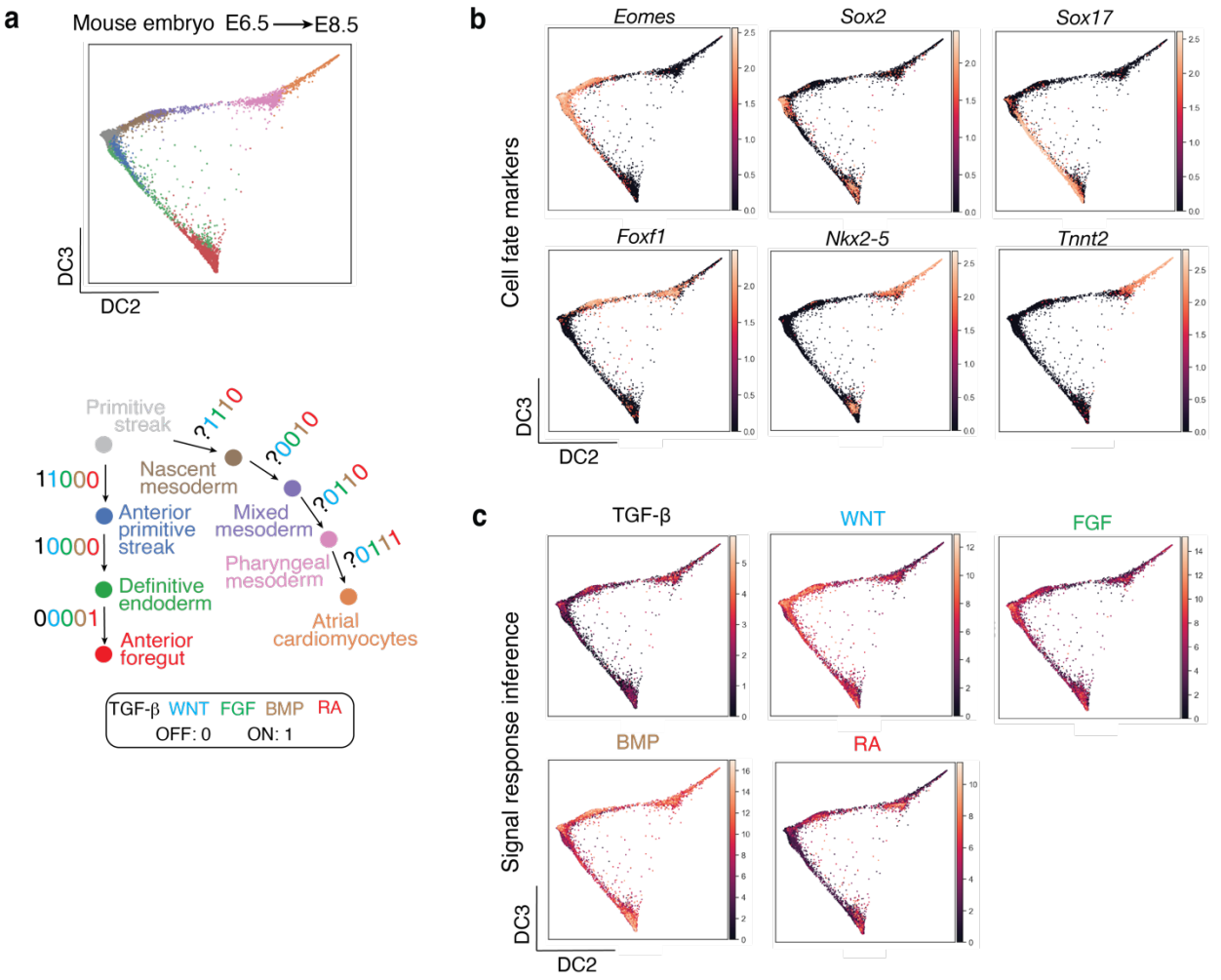

Supplementary Figure 2. Signal inference of *in vivo* cell types using the response-gene method. **a**, Construction of the anterior foregut and atrial cardiomyocyte trajectories, using cell populations from the mouse embryo (E6.5-E8.5) scRNAseq dataset [35]. The colors of the cell populations in the diffusion map correspond to those in the schematic. Signal combinations at each step of differentiation were annotated based on the literature. Due to lack of knowledge in the literature, the activity of TGF-β along the cardiac lineage was left out in the annotation. **b**, The expression of key cell fate markers associated with each of the two lineages (normalized to counts per 10^4). **c**, Signal response-gene scores for all five signaling pathways. Consistent thresholds for binary classification from these scores are difficult to calibrate, limiting their interpretability.

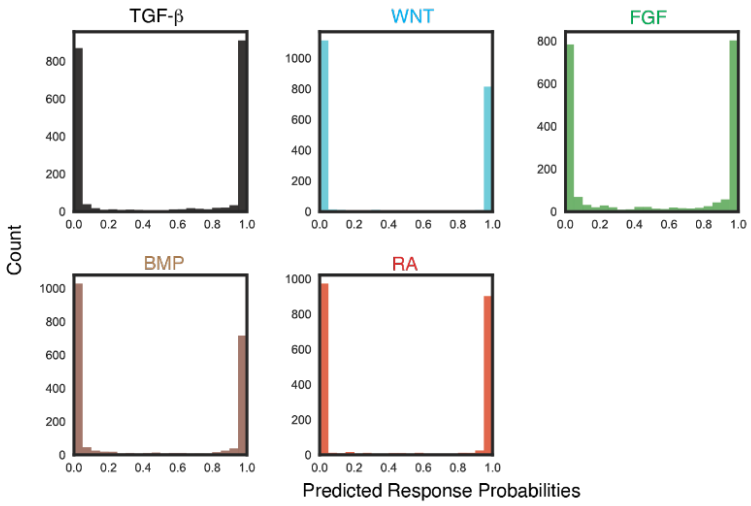

Supplementary Figure 3. Distribution of IRIS predicted response probability and thresholding. IRIS predicted response probability values were close to 0 and 1 in the in-sample test using mouse screen data, potentially due to the saturation concentrations of ligands used in the screen. 0.5 was chosen as the threshold for the model to be agnostic to the types of downstream errors.

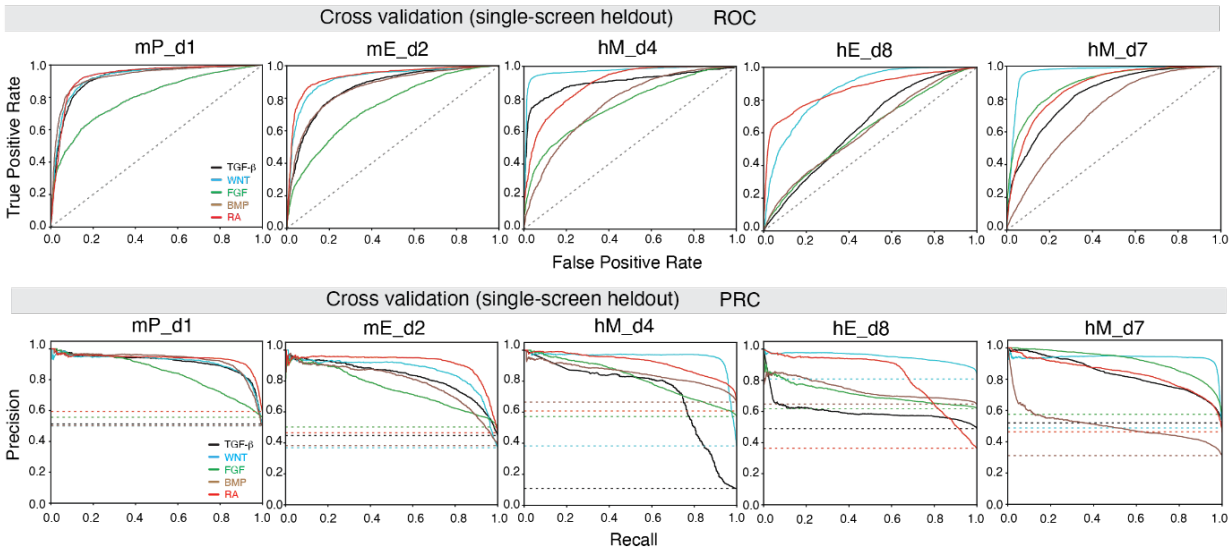

Supplementary Figure 4. Model evaluation via a cross-validation test.
The AUROC (*top*) and PRC (*bottom*) curves of the cross-validation test, with a single screen held out each time (related to Fig. 2c). A random baseline for each pathway (*dashed lines*) was used for comparison.

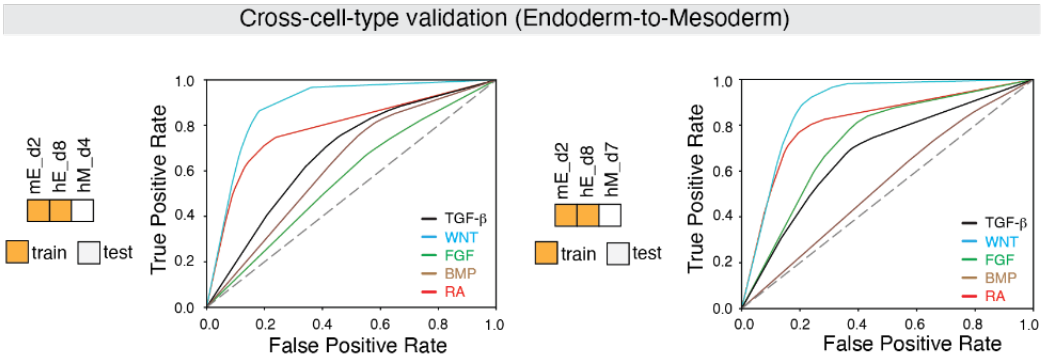

Supplementary Figure 5. Evaluating cross-cell-type generalization.
The AUROC curves of the cross-cell type generalization test, in which IRIS was trained on two endodermal screens (mE_d2, hE_d8) and tested on mesodermal screens (hM_d4, hM_d7) (related to Fig. 2d)

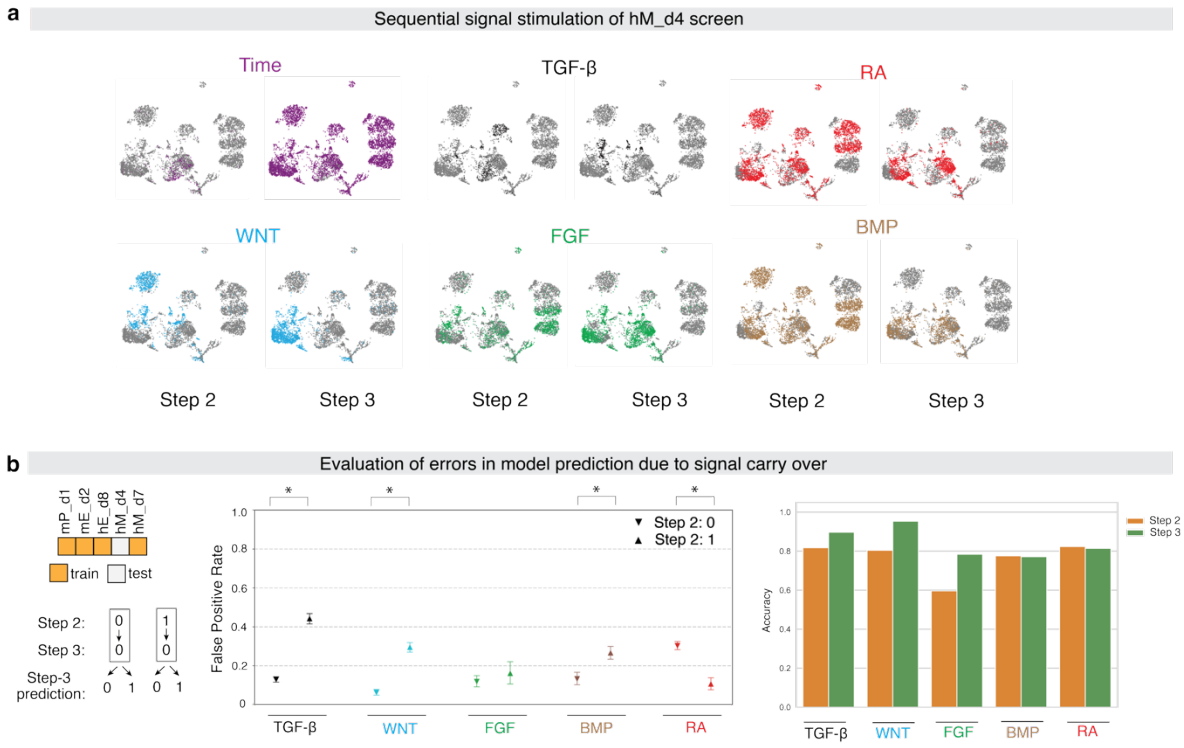

Supplementary Figure 6. Evaluation of signaling carry-over across time steps.
a, Ground-truth signaling labels for the hM_d4 screen. Cells with the signaling pathway activated during Step 2 (*left*) or Step 3 (*right*) are shown separately, and they are highlighted in the corresponding color on the UMAP plots. The "Time" UMAP plots highlight the cells that were sequenced after Step 2 or Step 3 stimulation separately. **b,** Evaluation of false positive rates (FPR) in model prediction due to signal carry-over. *Left:* For each signaling pathway, the FPR in Step 3 was calculated for cells that had received the same signal in Step 2 and compared against cells that had not received the same signal in Step 2. 95% confidence intervals were determined using bootstrapping of n=1000 samples. The center is the mean false positive rate. Two-tailed z-test with standard errors (n=3903; * indicates $p < 0.05$). *Right:* Comparing model accuracy on cells that were only treated with 2-steps of signal combination vs cells that were treated with 3-steps of signal combination.

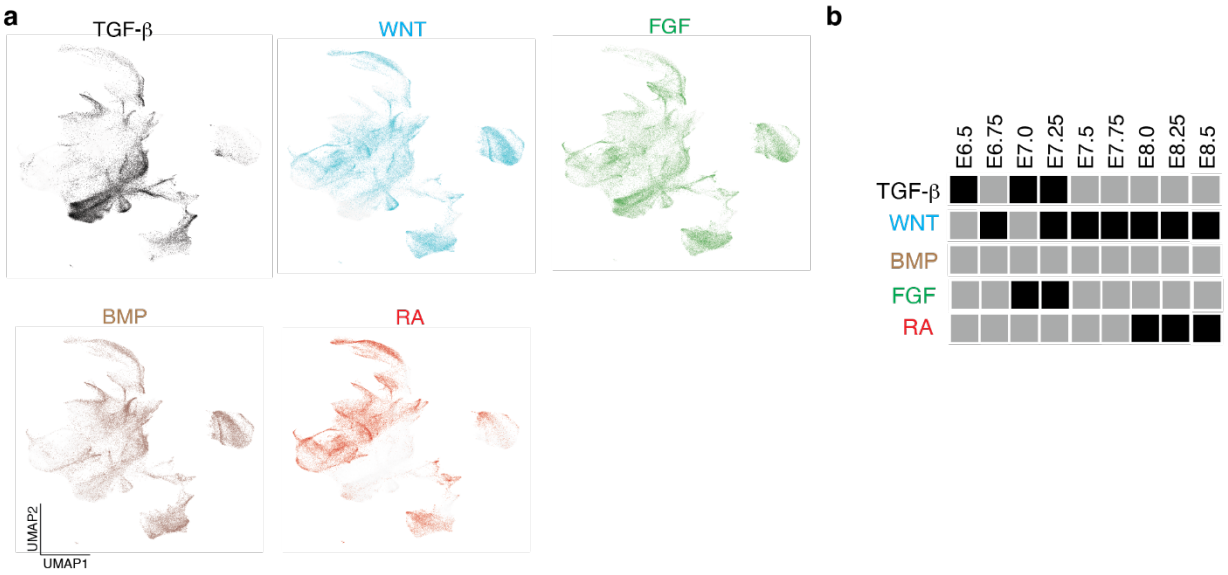

Supplementary Figure 7. Inferring the activity of individual signaling pathways across the mouse gastrulation dataset.
a, The five signaling pathway activation predictions annotated on the mouse gastrulation atlas revealed patterns of response across diverse cell types. Cells inferred to have the denoted signaling pathway activated are highlighted in the corresponding color. **b,** Enrichment of signaling pathway activation across stages of embryonic development. Black squares denote significant enrichment via a one-tailed Mann Whitney u-test (n=139331; $p < 0.05$) (alternative: greater). See Supplementary Table 1 for p-values.

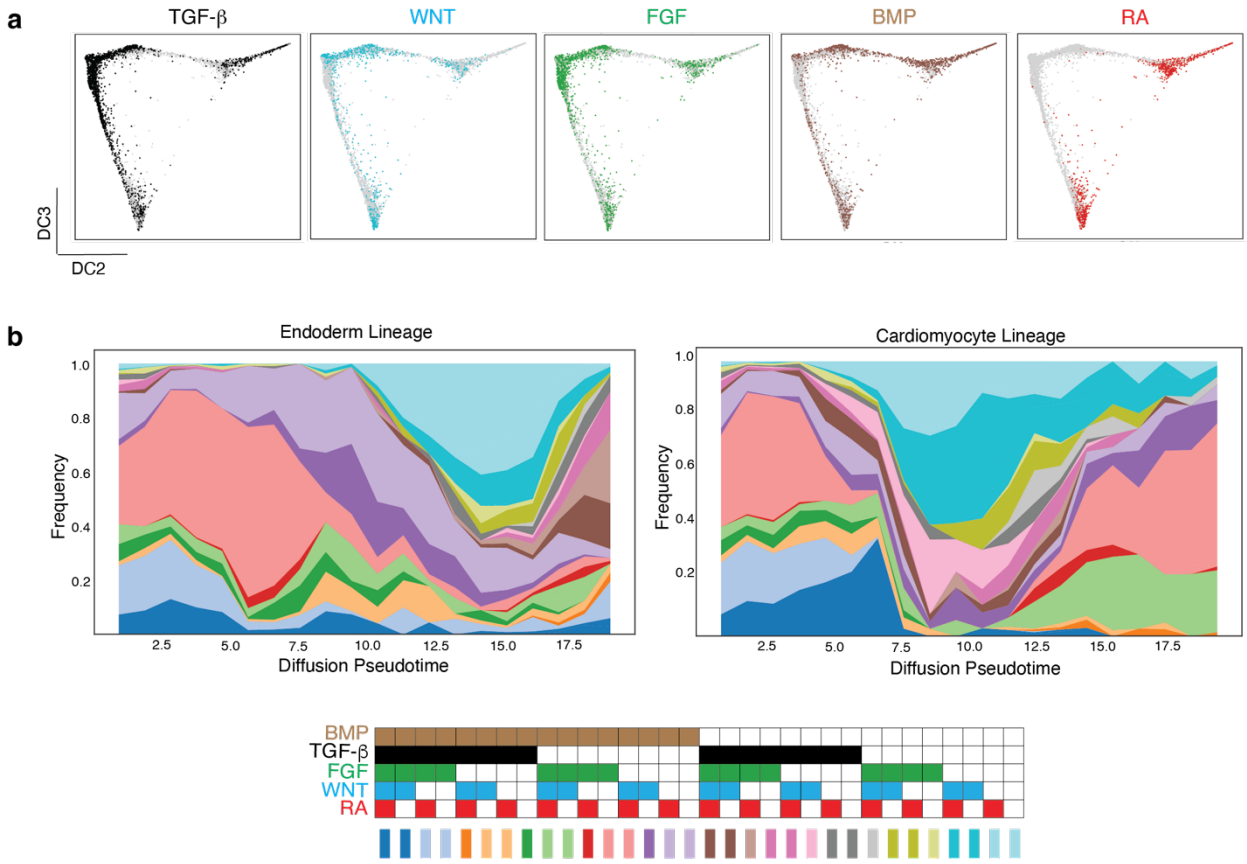

Supplementary Figure 8. IRIS prediction for the endodermal and cardiac lineages.
a, Inferred signaling states for individual pathways across both the endodermal and cardiac lineages. Cells are arranged in the same way as they are in **Fig. 3c**. Cells inferred to have the denoted signaling pathway activated are highlighted in the corresponding color. **b**, Frequencies of all inferred signal combinations among the 5 pathways across the inferred pseudotime.

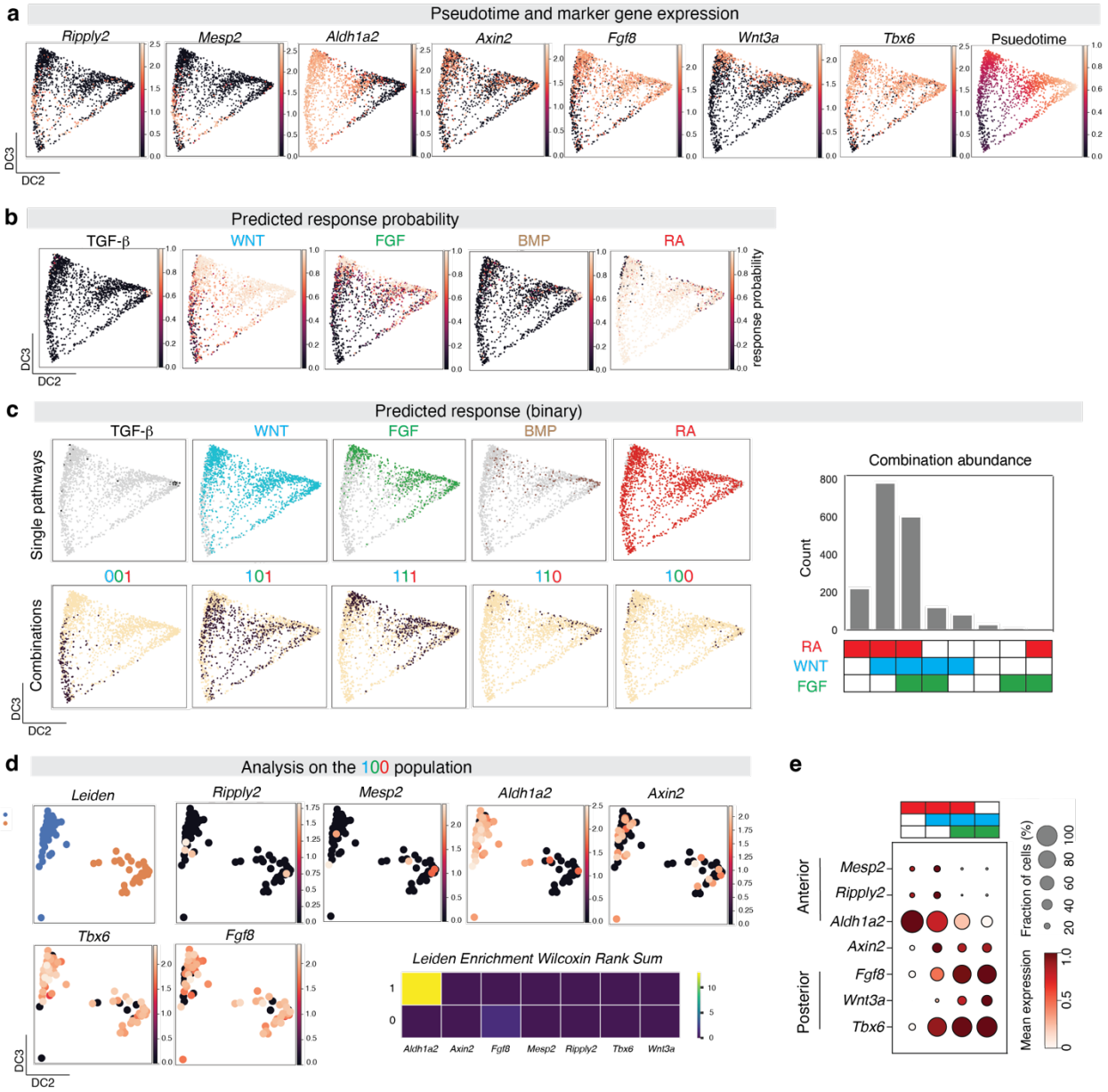

Supplementary Figure 9. Spatial reconstruction of heterogeneous signaling states among somitic mesoderm cells.

a, Expression of marker genes that are associated with spatial positions of the cells in the somitic mesoderm (n=2079) plotted on a diffusion map (Anterior: *Ripply2, Mesp2, Aldh1a2*; Posterior: *Tbx6, Wnt3a, Fgf8*; Signaling State: *Axin2*). **b,** Predicted response probability for each signaling pathway on the somitic mesoderm population annotated in the atlas. **c,** Binary predictions of pathway activation and their combinations (*left*). Counts of cells annotated with each signal combination, with top five combinations accounting for 99.5% of the cells (*right*). **d**, Re-clustering of the predicted WNT+FGF-RA- cells show two distinct clusters with either anterior or posterior identities, suggesting WNT+FGF-RA- cells are most likely a collection of cells with false-negative and/or false-positive annotation of the signaling states. **e,** Differential enrichment of marker genes associated with spatial positions among inferred subpopulations of the somitic mesoderm, including RA+WNT-FGF- (*Ripply2, Mesp2, Aldh1a2),* RA+WNT+FGF- (*Aldh1a2, Tbx6)*, RA+WNT+FGF+ (*Wnt3a, Fgf8, Tbx6*), and RA-WNT+FGF+ (*Wnt3a, Fgf8, Tbx6*). One-

tailed Mann-Whitney U-test (alternative: greater) of each gene's expression in each subpopulation relative to all other subpopulations.

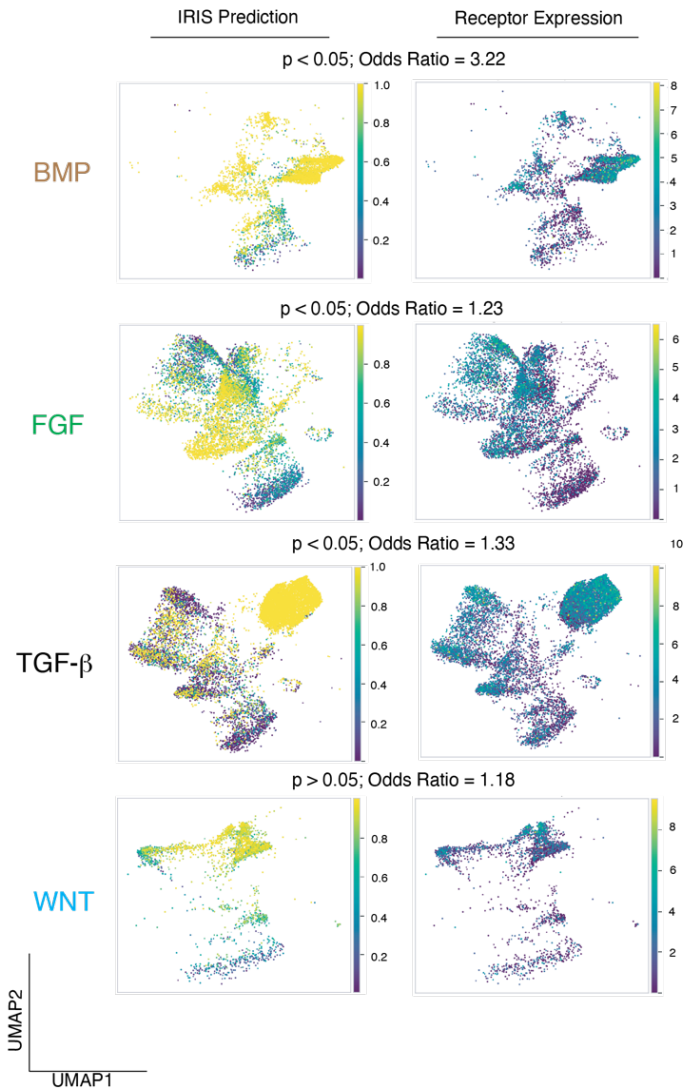

Supplementary Figure 10. IRIS signaling prediction on adult human airway epithelial cells.
IRIS predicted signaling response probabilities on adult human airway epithelial cells, which have been stimulated with the respective ligands for 7 days (*left*). The stimulation includes BMP (BMP4; n=3891), FGF (FGF2 and FGF10; n=7053), TGF-β (TGF-β2 and Activin A; n=11084), and WNT (chemical agonist CHIR; n=2643) [43]. Summed expression levels of the corresponding receptor families for each pathway in counts-per-million (CPM) (*right*). Cells predicted to be activated by the signaling pathway were significantly enriched among cells with detectable levels of the corresponding receptor expression ($p < 0.05$; two-tailed Fischer's exact test) except for cells treated with CHIR, which bypasses receptors to directly activate the intracellular signal transduction of the WNT pathway. The odds ratio shows the strength of a statistically significant relationship. Note that using receptor expression to approximate signaling potential could lead to false negatives due to dropouts of lowly expressed receptors.

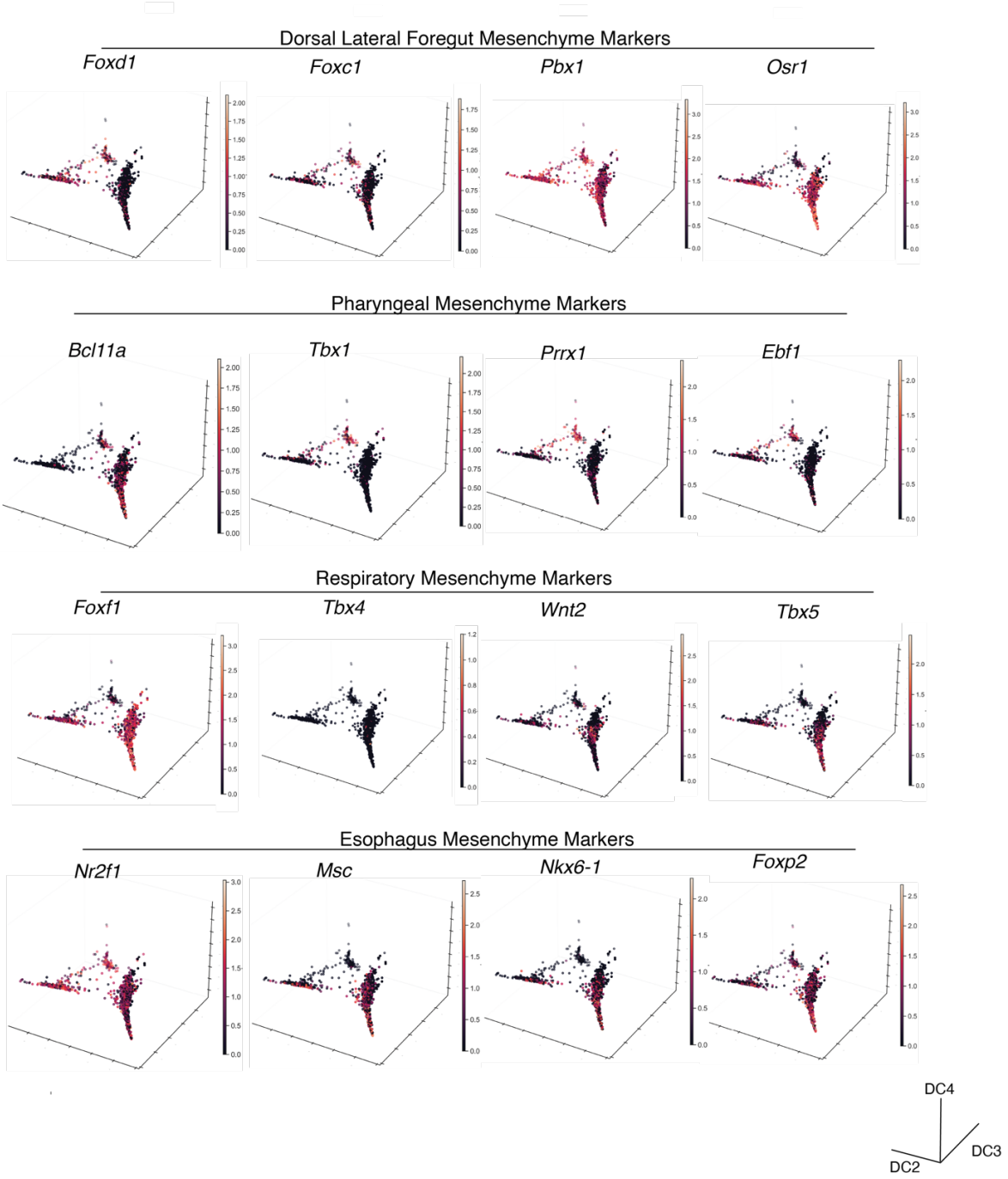

Supplementary Figure 11. Fate divergence of organ-specific mesenchyme.
Marker genes corresponding to the dorsal lateral foregut mesenchyme, esophageal, pharyngeal and respiratory mesenchyme are overlaid on the diffusion maps. The respective cell populations are from E9-E9.5 mouse embryo foregut [17], and the 3D diffusion map was constructed in **Fig. 4a**.